Astronomy
&
Astrophysics

Time-resolved spectroscopy of the roAp star γ Equ[⋆]

O. Kochukhov[1] and T. Ryabchikova[2,3]

[1] Uppsala Astronomical Observatory, Box 515, 751 20 Uppsala, Sweden
[2] Institute of Astronomy, Russian Academy of Sciences, Pyatnitskaya 48, 109017 Moscow, Russia
   e-mail: ryabchik@inasan.rssi.ru
[3] Institute for Astronomy, University of Vienna, Türkenschanzstrasse 17, 1180 Vienna, Austria
   e-mail: ryabchik@tycho.astro.univie.ac.at

Abstract. We report results of the spectroscopic monitoring of the roAp star γ Equ with the ESO 3.6-m telescope. During 1.5 hours of observations a series of very high-resolution and high S/N spectra was obtained for this star in the 6138–6165 Å spectral region. Short exposure times allowed us to resolve changes of γ Equ line profiles due to the rapid pulsations and to follow profile variations over 5 oscillation cycles. From this unique observational material information on amplitudes and phase shifts of radial velocity (RV) variations was extracted for 29 lines of 17 individual ions. We confirmed that spectral lines of rare-earth elements (REE) have the largest pulsation amplitudes, reaching up to 0.8 km s^{-1}. Moreover, we detected a phase shift between RV variations of singly and doubly ionized REE, discovered significant RV shifts of weak Na I lines and analysed line profile variations of Pr III and Nd III spectral features. This rich observational material opens a possibility to obtain a detailed picture of the vertical stratification of chemical elements and extract the main characteristics of the pulsational mode(s). In our observations we did not find support for the existence of the unique dependence of RV amplitude on line strength suggested in earlier spectroscopic studies of roAp stars. Instead, we argue that the individuality of the variations of all ions is a result of the complex interplay between inhomogeneous vertical and horizontal distributions of chemical elements and individual pulsation modes of γ Equ. We show that the extra line broadening observed in γ Equ spectrum is most likely caused by pulsations. A detailed analysis of Pr III and Nd III line profile variations resulted in the estimate of $\ell = 2$ or 3, $m = -\ell$ or $-\ell + 1$ and $v_{\rm p} \approx 10$ km s^{-1} for the p-mode of the main pulsation frequency.

Key words. stars: chemically peculiar – stars: oscillations – stars: individual: γ Equ

1. Introduction

Since the discovery of the short-period light variations in cool Ap star HD 101065 (Kurtz & Wegner 1979) this phenomenon became an object of interest for many studies. At present the group of rapidly oscillating Ap (roAp) stars consists of 32 members. These stars oscillate with periods in the range of 4–16 min and very low amplitudes ($\Delta B \leq 15$ mmag). γ Equ is the second brightest roAp star. The latest extensive analysis of its light variation from multi-site observations (Martinez et al. 1996) provides support for p-modes with four pulsation frequencies corresponding to periods from 11.68 to 12.45 min. Libbrecht (1988) was the first who found radial velocity variations with an amplitude of 42 m s^{-1} and with two out of four photometric periods: 12.20 and 11.68 min. Kanaan & Hatzes (1998) performed an extensive study of the radial velocity variations due to pulsations in γ Equ based

on high-precision echelle spectroscopy with an iodine cell. They found RV amplitudes ranging from 30 to 1000 m s^{-1} as measured from individual lines and concluded that the pulsational amplitudes depend on chemical species and are higher for weaker lines of the same element. Practically at the same time Malanushenko et al. (1998) published results of RV analysis of the individual lines in the 6112–72 Å spectral region. They discovered the highest RV amplitudes, up to 800 m s^{-1}, for the lines of Pr III and Nd III, while most other strong and weak lines in this region did not show amplitudes exceeding the accuracy of the RV measurements ($\approx$100 m s^{-1}). Malanushenko et al. (1998) found that the main frequency of RV pulsations, 1365 μHz (12.21 min), coincides with one of the photometric frequencies. Later Savanov et al. (1999) showed that some lines from the spectral regions for which Kanaan & Hatzes (1998) found large RV variations were not identified properly and in reality belong to singly and doubly ionized Pr and Nd.

γ Equ is the slowest known rotator among Ap stars. Its rotational period, $P = 77 \pm 10$ yr, was determined from published longitudinal magnetic field measurements

[⋆] Based on observations obtained at the European Southern Observatory, La Silla, Chile.
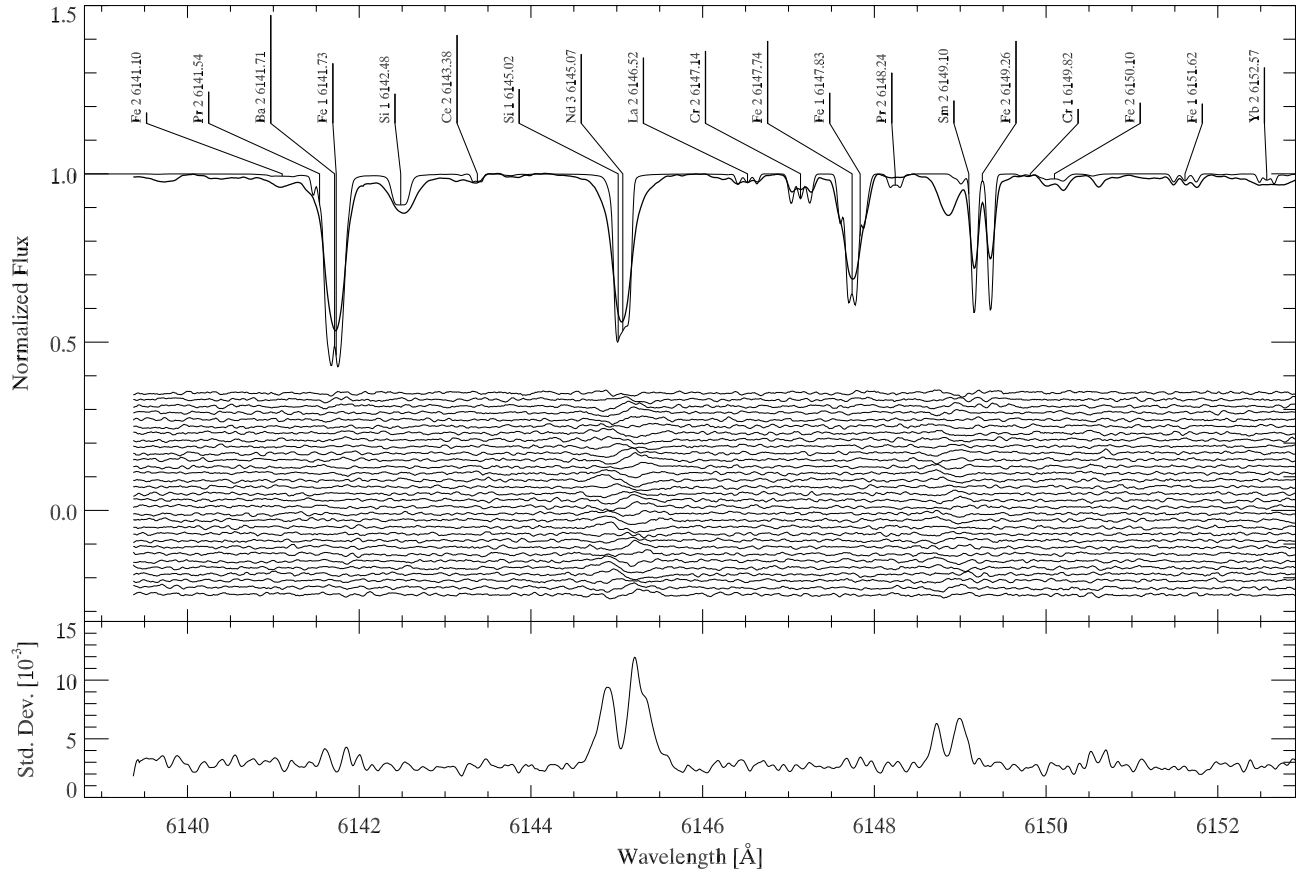
Fig. 1. A comparison between spectrum synthesis calculations (thin curve) and average spectrum of γ Equ (thick curve) is shown in the upper panel. The middle panel displays the difference between individual and average observed spectra. The profiles of the consecutive pulsation phases are shifted in the vertical direction by 0.02; the lower panel shows the standard deviation for each pixel of the observed spectrum.

by Leroy et al. (1994). Due to its extremely low rotational velocity we cannot observe any line profile variations connected with the surface abundance inhomogeneity typical for Ap stars. However, the short-term spectroscopic variability of γ Equ may be caused by non-radial oscillations. We obtained time-series of high-resolution high S/N spectra of γ Equ to study in detail the line profile variations due to stellar pulsations.

The observational data and reduction procedure are described in Sect. 2. Line identification and spectrum synthesis details are discussed in Sect. 3. We present the results of RV measurements in Sect. 4, while an analysis of REE line profile variations and an attempt of mode identification are given in Sect. 5. In Sect. 6 we discuss the pulsational broadening of the time-averaged γ Equ spectrum.

2. Observations and spectra reduction

The observations of γ Equ were collected in July 1999 in the backup programme of an observing run devoted to the investigation of magnetic fields on M-dwarf stars. We used the Very Long Camera of the Coude Echelle Spectrograph, fibre-linked with the Cassegrain focus of the ESO 3.6-m telescope. The combination of the third (highest resolu-

tion) CES image slicer and ESO CCD#38 provided a resolving power of $\lambda/\Delta\lambda \simeq 170\,000$. The observations of γ Equ were carried out for 1.5 hours. During that time we obtained 31 60^s exposures of a 26 Å spectral region centred at λ 6152 Å. The first spectrum was obtained at the heliocentric Julian date $\mathrm{HJD}_1 = 2451381.783444$, while the last one was acquired at $\mathrm{HJD}_{31} = 2451381.823897$. A signal-to-noise ratio of 130 was achieved in each individual exposure. A Th-Ar comparison spectrum was registered immediately before and after the observations of γ Equ.

The basic steps of spectra reduction (bias subtraction, flat field correction, extraction of 1D spectra and wavelength calibration) were performed with the set of IDL-based routines, specially adapted for the reduction of CES spectra. We used 12 emission lines in each of the Th-Ar comparison spectra in order to establish the wavelength scale. The positions of the emission lines were determined by fitting a Gaussian to the line profiles. Then a second order polynomial was used to fit the pixel-wavelength relation. This procedure allowed us to establish the wavelength scale with an internal accuracy of $\sim 5 \times 10^{-5}$ Å. We found a shift of 22 m s^{-1} between Th-Ar spectra taken before and after observations of γ Equ. By comparison, during 1.5 hours of observations the heliocentric radial velocity of the observing site changed by 113 m s^{-1} in the
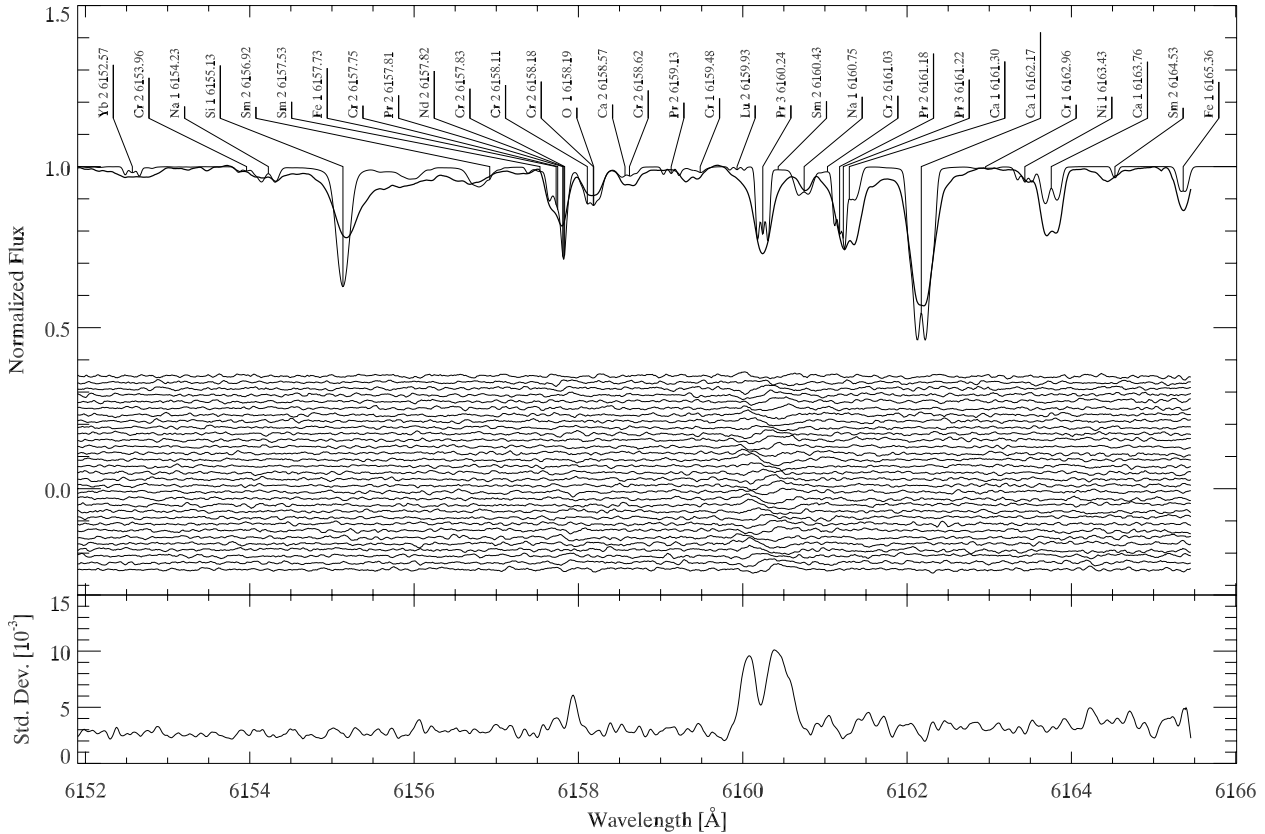
Fig. 1. continued.

direction towards the star. However, in order to simplify the spectroscopic analysis, no correction for the drift of the zero velocity point was made at this stage of the reduction, and an average dispersion relation was used for all 31 spectra. Instead we took into account the linear drift of the spectrograph reference frame when fitting radial velocity variations of the individual spectral lines (Sect. 4).

The average instrumental profile was determined from the same 12 Th-Ar emission lines that were used for the construction of the wavelength scale. The instrumental profile is well approximated with a Gaussian, corresponding to a resolving power of $\lambda/\Delta\lambda = 166\,000$. We found no evidence for a temporal variation of the instrumental profile or a systematic change in the dispersion direction.

In the final stage of the spectrum reduction special care was taken in order to achieve a consistent continuum normalization of the individual spectra. With the help of spectrum synthesis we selected a subset of spectral regions, free of strong lines, and then iteratively fitted a cubic polynomial through the continuum points, rejecting points with a large deviation from the provisional continuum level. Then we inspected the difference between each individual and the average spectrum (Fig. 1) and modified the selection of the line-free regions until large-scale deviations of individual spectra from the average were removed.

3. Spectrum synthesis and line identification

For the purpose of line identification and determination of the mean stellar RV we computed a synthetic spectrum of γ Equ in the 6140–6166 Å spectral region. Model atmosphere parameters, an approximate model of the magnetic geometry, and elemental abundances were adopted from Ryabchikova et al. (1997). All relevant atomic parameters were extracted from the VALD database (Kupka et al. 1999). The oscillator strengths of Ca I 6162.17, 6163.76 Å lines and Si I 6142.48, 6145.02, 6155.13 Å lines were further tuned by fitting the solar atlas of Kurucz et al. (1994). For the spectral lines of Pr III oscillator strengths were kindly provided to us by D. Bord (private communication). Synthetic spectra were calculated with the `Synthmag` magnetic spectrum synthesis code (Piskunov 1999), which makes it possible to obtain an accurate numerical solution of the polarised vector radiative transfer equation, and evaluate local Stokes profiles for a number of limb angles. Then an external IDL subroutine was used to obtain disk-integrated normalized spectra for a given macroturbulent and rotation velocity under the assumption of a homogeneous surface magnetic distribution. Although the latter simplification is generally not adequate for the explanation of the polarisation properties and variability of the radiation from Ap stars, it still provides a robust estimate of the Zeeman effect in the unpolarised line profiles of the slowly rotating Ap stars.

The line identification in 6140–6166 Å region is fairly complete. The only relatively strong unidentified spectral

feature is located at λ 6148.86 Å and probably belongs to the singly or doubly ionized REE (see Savanov et al. 1999 and Sect. 4). The Nd III 6145.07 Å line is blended with the line of Si I 6145.02 Å and the latter may contribute up to 25% to the total intensity of the observed feature.

A comparison between the spectrum synthesis and the average observed spectrum of γ Equ ($S/N \simeq 700$) is illustrated in Fig. 1. In the calculations we assumed that the atmosphere of the star is locally stabilized by the magnetic field, and therefore no micro or macro-turbulent broadening was introduced into the spectrum synthesis. Similarly, rotational broadening of the γ Equ spectra should be negligible due to the very long rotation period of the star. Thus, the only broadening effects that we expect are due to the magnetic field and the finite instrumental resolution. Nevertheless, the upper panel of Fig. 1 shows that the synthetic spectrum, convolved with a Gaussian profile ($FWHM = 37$ mÅ) to account for the instrumental broadening, still possesses much sharper spectral features than those seen in the observed spectrum. This excessive broadening cannot be ascribed to real macroturbulent or microturbulent motions, or to spurious instrumental smearing[1]. In fact, we did not find any combination of these effects that could simultaneously fit wide wings of the strong lines (such as Ba II 6141.71 Å, Nd III 6145.07 Å, and Ca I 6162.17 Å) and not wipe out the partially resolved Zeeman structure of the weaker lines (La II 6146.52 Å, Cr II 6147.14 Å, and Fe I 6151.62 Å). On the other hand, the separation of the Zeeman components of Fe II 6149.26 Å is well reproduced in our calculations. This suggests that the discrepancy between observations and spectrum synthesis cannot be explained by an underestimate of the mean field modulus in our model of the magnetic topology.

Stratification of chemical elements in the stellar atmosphere is one of the effects that may be responsible for the peculiar shape of the line profiles in the spectrum of γ Equ. Diffusion theory (Michaud 1970), which is the leading theoretical framework for the explanation of the abundance anomalies of Ap and related stars, predicts that in stellar atmospheres, stabilized by kilogauss magnetic fields, radiation pressure and gravitational settling will gradually build up a superficial layer with a peculiar chemical composition. Detailed diffusion calculations by Babel (1992) suggested that strong vertical abundance gradients can be expected within the line forming regions. In particular, elemental concentrations of Ca and iron-peak elements feature similar vertical distributions consisting of the layer with enhanced abundance, located at the bottom of the

---

[1] Admittedly the average spectrum of γ Equ was constructed by direct coaddition of the individual exposures, without taking into account small relative shifts of the individual spectra due to the Earth motion and spectrograph drift. However, the RV shift of 135 m s^{-1} between the first and the last exposure corresponds to only 2.8 mÅ and is negligible in comparison with $FWHM$ of the instrumental profile.

atmosphere, and the layer with solar (or even less than solar) abundance above optical depth $\log \tau_{5000} = -1$. In this scheme the spectral lines of stratified chemical elements will tend to have weaker cores and wider wings relative to line profiles calculated under the assumption of an homogeneous vertical distribution.

Numerical tests confirmed that introducing vertical stratification can in principle improve the fit to the observed line profiles. It also allows us to achieve consistency in the abundances, derived from the spectral lines of different ionization stages of the same elements as well as weaker and stronger lines of the same ions. However, in our preliminary calculations we could not find a unique vertical chemical abundance distribution that can account for both abnormal profiles *and* strength of doubly ionized REE lines. This has to be confirmed by detailed quantitative investigation of the vertical stratification in γ Equ which is outside the scope of the present paper.

An effect of stellar pulsation on line broadening will be discussed in Sect. 6.

From the shift between the synthetic and average observed spectrum we found that the mean radial velocity of γ Equ is -16.87 km s^{-1}, which is in good agreement with other recent determinations (Mkrtichian et al. 1998).

4. Analysis of radial velocity variations

In the first step of the analysis of pulsational changes in γ Equ line profiles we computed the difference between the average and 31 individual spectra and determined a standard deviation for each pixel of the observed spectral region. Prominent variations of Nd III 6145.07 Å and Pr III 6160.24 Å are immediately seen in the difference spectra (middle panel in Fig. 1). *This is the first clear detection of metal line profile variability due to the rapid oscillation in a roAp star.* Analysis of the standard deviation (lower panel in Fig. 1) reveals weaker variability in other spectral lines, such as Ba II 6141.71 Å, unidentified features at 6148.86 and 6150.62 Å, and a complex blend at 6157.8 Å, containing several spectral lines of REE. The shape of the standard deviation profiles for Nd III and Pr III spectral lines is very similar to the variability of spectral features in non-radially pulsating δ Scuti and β Cep stars (Mantegazza 2000).

We took a closer look at the variability of γ Equ spectral lines by measuring the radial velocity shifts of each individual spectral feature. The positions of the spectral lines were determined with the help of the center-of-gravity method:

$$\lambda_{\mathrm{c}}^{j} = \sum_i \lambda_i (1 - f_i^j) / \sum_i (1 - f_i^j), \qquad (1)$$

where f_i^j is the residual flux in the ith pixel of the normalized spectrum and the index j refers to the temporal sequence of our observations ($j = 1, \ldots, 31$). Then the wavelength shifts were transformed to the RV scale
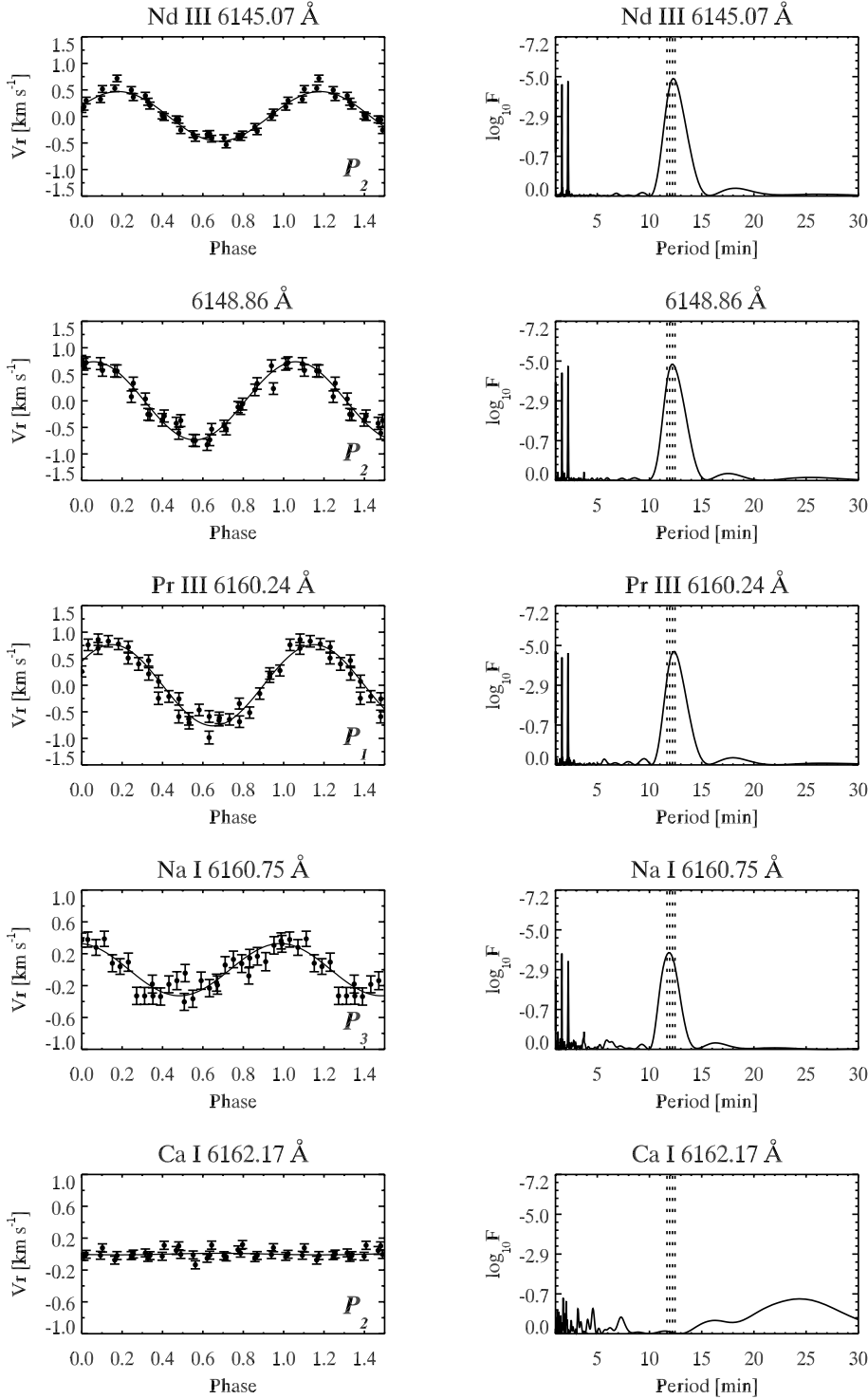
Fig. 2. RV curves of selected spectral lines are shown in the left panels. The solid curve is the best-fit cosine curve. The photometric period which was adopted for this fit is indicated in the lower left corner of each RV panel. The right panels show periodograms $F(P)$, where F is the probability that the variation with a given period is a noise artifact. Vertical dotted lines mark the photometric pulsational periods of γ Equ.

relative to the average centroid wavelength $\langle \lambda_c \rangle$

$$V_c^j = \frac{c}{\langle \lambda_c \rangle} \left(\lambda_c^j - \langle \lambda_c \rangle \right). \qquad (2)$$

RV determined in this way proved to be stable and accurate characteristic of spectral line position. An alternative method, such as fitting analytical profiles to the lines in the observed spectra, is not applicable for the analysis of the complex profiles of spectral lines altered by magnetic broadening or splitting. On the other hand,

measuring RV shifts by cross-correlation with the average spectrum reduces to the problem of finding the maximum or center-of-gravity of the cross-correlation function and therefore is equivalent to the direct analysis of individual spectral lines. Besides, centroid RV has the advantage of being a special case of a more general moment technique (see Sect. 5.1), which proved to be very useful in the spectroscopic analysis (in particular mode identification) of non-radially pulsating stars.

Table 1. Radial velocity variations of individual spectral lines. Phases φ are expressed in units of the period. Arabic numerals mark the main components of unresolved blends.

Ion	λ_{lab} Å	K $\mathrm{m\,s^{-1}}$	σ_{K} $\mathrm{m\,s^{-1}}$	φ	σ_φ	P
Fe II	6141.10	$\leq$120				
Ba II	6141.71	93	16	0.899	0.031	2,3
Si I	6142.48	$\leq$90				
Ce II	6143.38	296:	60	0.915:	0.034	2,1
Nd III	6145.07[1]	470	21	0.159	0.007	2,1
Si I	6145.02[1]					
La II	6146.52	216:	49	0.944:	0.039	2,3
Cr II	6147.14	$\leq$60				
Fe II	6147.74	72:	16	0.674:	0.037	3,4
Pr II	6148.24	348	96	0.886	0.048	2
uncl.	6148.86	736	30	0.060	0.006	2
Fe II	6149.26	64:	14	0.667:	0.036	3,4
Fe II	6150.10	89:	35	0.473:	0.073	4,3
uncl.	6150.62	557	44	0.141	0.044	3,2
Fe I	6151.62	$\leq$75				
Yb II	6152.57	377:	95	0.881:	0.045	4,3
Na I	6154.23	364	72	0.893	0.032	3,4
Si I	6155.13	$\leq$70				
Sm II	6156.92	320	50	0.953	0.025	2,3
Fe I	6157.73[2]	209:	17	0.039:	0.013	2,3
Nd II	6157.82[2]					
Cr II	6158.11[3]	184	31	0.564	0.027	1,2
Cr II	6158.18[3]					
O I	6158.18[3]					
Ca II	6158.57[4]	137	47	0.056	0.052	1,2
Cr II	6158.62[4]					
Fe I	6159.38[5]	$\leq$100				
Cr I	6159.48[5]					
Pr III	6160.24	788	37	0.169	0.007	1,2
Na I	6160.75	320	30	0.958	0.016	3,4
Pr II	6161.18[6]	339	33	0.151	0.016	1,2
Pr III	6161.22[6]					
Ca I	6161.30[6]					
Ca I	6162.17	$\leq$30				
Ca I	6163.76	$\leq$35				
Sm II	6164.53[7]	446	56	0.926	0.022	1,2
Ce II	6164.41[7]					
Fe I	6165.36	$\leq$50				

For the measurements of line positions we usually selected the unblended part of the profiles. RV shifts of a few weak lines (Fe II 6141.10 Å and Na I 6160.75 Å), situated in the wings of strong spectral features, were also determined. The resolved Zeeman components of Fe II 6149.26 Å were analysed separately and the results were averaged, but for all other weaker features with partially resolved Zeeman structure (La II 6145.52 Å, Cr II 6147.14 Å, Fe II 6150.10 Å, and Fe I 6151.62 Å) we determined common line centers.

The errors of centroid RV measurements were found from a formal error estimate, which follows from Eq. (1)

$$\sigma^2(V_c) = \frac{c^2}{\lambda_c^2} \sum_i \sigma^2(f_i) \left(\frac{\lambda_i - \lambda_c}{\sum_k f_k} \right)^2, \qquad (3)$$

where the uncertainty $\sigma(f_i)$, ascribed to the ith pixel of normalized spectrum, is found from the Poisson photon statistics. In addition, a useful independent estimate of $\sigma^2(V_c)$ was found by simulating the process of center-of-gravity measurements. This was done by adding random noise to the average spectrum and determining λ_c. The whole procedure was repeated 30–40 times with different noise realisations and the resulting standard deviation for λ_c was determined. Both the formal error estimate (3) and Monte-Carlo simulations gave typical uncertainty of 20–50 $\mathrm{m\,s^{-1}}$ for RV measurements of strong lines, while errors in the RV determination reach 100–200 $\mathrm{m\,s^{-1}}$ for weak lines. These error estimates agree well with the standard deviation of individual radial velocity measurements from the best-fit cosine curves.

From the time-series of radial velocity measurements we computed periodograms using the method of Horne & Baliunas (1986). Since spectroscopic monitoring of γ Equ was carried out for only 1.5 hours and we had 31 consecutive RV measurements for each spectral line, we could not determine the pulsation period with good accuracy and distinguish pulsation frequencies found in previous photometric studies of γ Equ (Martinez et al. 1996). Nevertheless, useful information about the *probability* of variation with a certain frequency was obtained from the periodogram analysis (right panels in Fig. 2).

For each line we fitted RV variations with a combination of a linear term (to account for spectrograph drift and Earth motion) and a cosine curve

$$V_c^j = V_0 + V_1 t^j + K \cos[2\pi(t^j/P + \varphi)], \qquad (4)$$

where K is the semi-amplitude of RV variations, φ is the phase shift, t^j is the time interval between the first and the jth exposure, V_0 and V_1 are constants, and P is the adopted period of pulsations. The constant V_1 was determined in the reduction procedure (Sect. 2) and was fixed at 3.863×10^{-2} $\mathrm{m\,s^{-2}}$, while V_0, K, φ and their errors were found with the help of the non-linear least-squares Marquardt method (Bevington 1969). A least-squares fit was carried out for each of the pulsation periods determined by Martinez et al. (1996) ($P_1 = 12.45, P_2 = 12.20, P_3 = 11.93, P_4 = 11.68$ min). The results of the analysis of RV variations are summarised in Table 1. For each spectral line or unresolved blend we give the identification, laboratory wavelength, semi-amplitude and phase of RV variation, as well as the corresponding error estimates. Although our observational data did not allow us to distinguish photometric pulsation frequencies on the basis of periodogram analysis, we found that fitting RV curves with different photometric periods resulted in different χ^2 of the fit. In particular, for lines with well defined RV curves the fit with the best out of four photometric periods resulted in a χ^2 which was a factor of 2–3 smaller than the value derived by adopting the worst period. Thus, we felt it useful to indicate in the last column of Table 1 the photometric period that corresponds to the lowest χ^2 of the fit. If χ^2 of the two best-fit periods did not differ
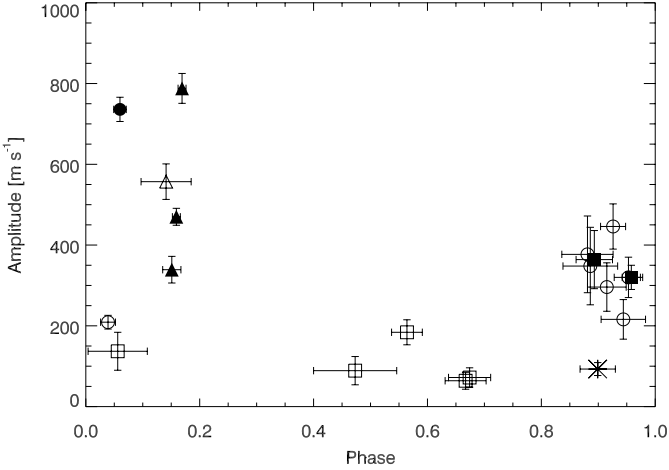
Fig. 3. Amplitude and phases of the RV variations of spectral lines and blends dominated by doubly ionized REE (filled triangles), singly ionized REE (open circles), Na I (filled squares), Ba II (asterisk) and iron-peak elements (open squares). Unidentified spectral lines are marked by filled circle (λ 6148.86 Å) and open triangle (λ 6150.62 Å).

by more than 30%, we listed both periods in order of increasing χ^2. For some spectral lines only upper limits of K could be determined, while for other spectral features K and φ strongly depend on the selection of the part of the line profile used for RV measurements, hence we marked these results as uncertain. Figure 3 displays the amplitudes and phases of RV curves for variable spectral lines.

Figure 2 shows examples of RV curves and periodograms, computed for Nd III 6145.07 Å, an unidentified feature at 6148.86 Å, Pr III 6160.24 Å, Na I 6160.75 Å, and Ca I 6162.17 Å. Savanov et al. (1999) already mentioned that the 6148.86 Å line shows high amplitude RV variations, and they proposed it belongs to the second ions of REE from the similarity of the RV amplitudes. Our detailed analysis of both RV amplitudes and phase shifts shows that the line may belong either to singly or to doubly ionized REE.

For the two strongest lines of doubly ionized REE we tried to determine the pulsation period directly by a non-linear fit of a sinusoid to the RV curve. We found $P = 12.25 \pm 0.05$ min for Nd III 6145.07 Å and $P = 12.35 \pm 0.05$ min for Pr III 6160.24 Å, while pulsational amplitudes and phase shifts did not change significantly in comparison with the values given in Table 1.

5. Profile variations of Nd III and Pr III spectral lines and mode analysis

5.1. Moments of line profiles

The variability of Nd III and Pr III spectral features can be conveniently quantified by considering time variations of a few low-order moments of a line profile. This observational material can then be used to identify frequencies and modes of non-radial stellar oscillations. The moment technique was first developed by Balona (1986a, 1986b),

then Aerts et al. (1992) extended and applied this method to line profile variations of the monoperiodic β Cep star δ Ceti. The moment method turned out to be the best mode identification technique for non-degenerate slowly rotating pulsators, and therefore it seems especially suitable for roAp stars.

To measure the first four moments we transformed the wavelength scale λ into velocity units v relative to the center-of-mass velocity, which is the zero point of the variation of the first moment. Then the nth order moment was computed as

$$\langle V^n \rangle^j = \sum_i v_i^n y_i^j / W_\lambda^j,$$
$$W_\lambda^j = \sum_i y_i^j, \tag{5}$$

where the zeroth order moment W_λ is just the equivalent width of the line and y_i^j is the flux in the ith pixel of the jth spectrum, normalized to the continuum and subtracted from unity ($y_i^j = 1 - f_i^j$). In order to obtain complete information about line profile variations we carried out the summation over the whole variable part of Nd III 6145.07 Å and Pr III 6160.24 Å line profiles, as determined from the standard deviation plot in the lower panels of Fig. 1.

Formal errors of the moment measurements were derived by applying the error propagation laws to formula (5):

$$\sigma^2 \langle V^n \rangle^j = \sum_i \left[\frac{\sigma(y_i^j)}{\sum_k y_k^j} (v_i^n - \langle V^n \rangle^j) \right]^2, \tag{6}$$

where $\sigma(y_i^j)$ is the uncertainty of the flux in the ith pixel of the jth spectrum.

Figure 4 illustrates the variations of the line profile moments of doubly ionized REE lines. Similar to the analysis of the centroid RV variations (Sect. 4), we used non-linear least-squares sinusoid fitting to find the amplitudes, phases and constant terms of the moment variations. Time-series of each moment were fitted with

$$\langle V^n \rangle^j = \overline{\langle V^n \rangle} + K_n \cos(2\pi t^j / P + \varphi_n), \tag{7}$$

where the moments are defined in such a way, that $\overline{\langle V^n \rangle}$ is non-zero only for the even moments. K_n and φ_n determined for each moment are listed in Table 2. According to the results of Sect. 4 we fixed the period P in the least-squares fit at $P_2 = 12.20$ min for Nd III 6145.07 Å and at $P_1 = 12.45$ min for Pr III 6160.24 Å.

From the theoretical expressions for the variation of the moments of line profiles of non-radially oscillating stars (Aerts et al. 1992) we expect the oscillation frequencies $2/P$ and $3/P$ to be present in the variation of the second and third moments. For γ Equ the rotation frequency Ω is negligible in comparison with the pulsation frequency ω. In this case the expressions of Aerts et al. (1992) for
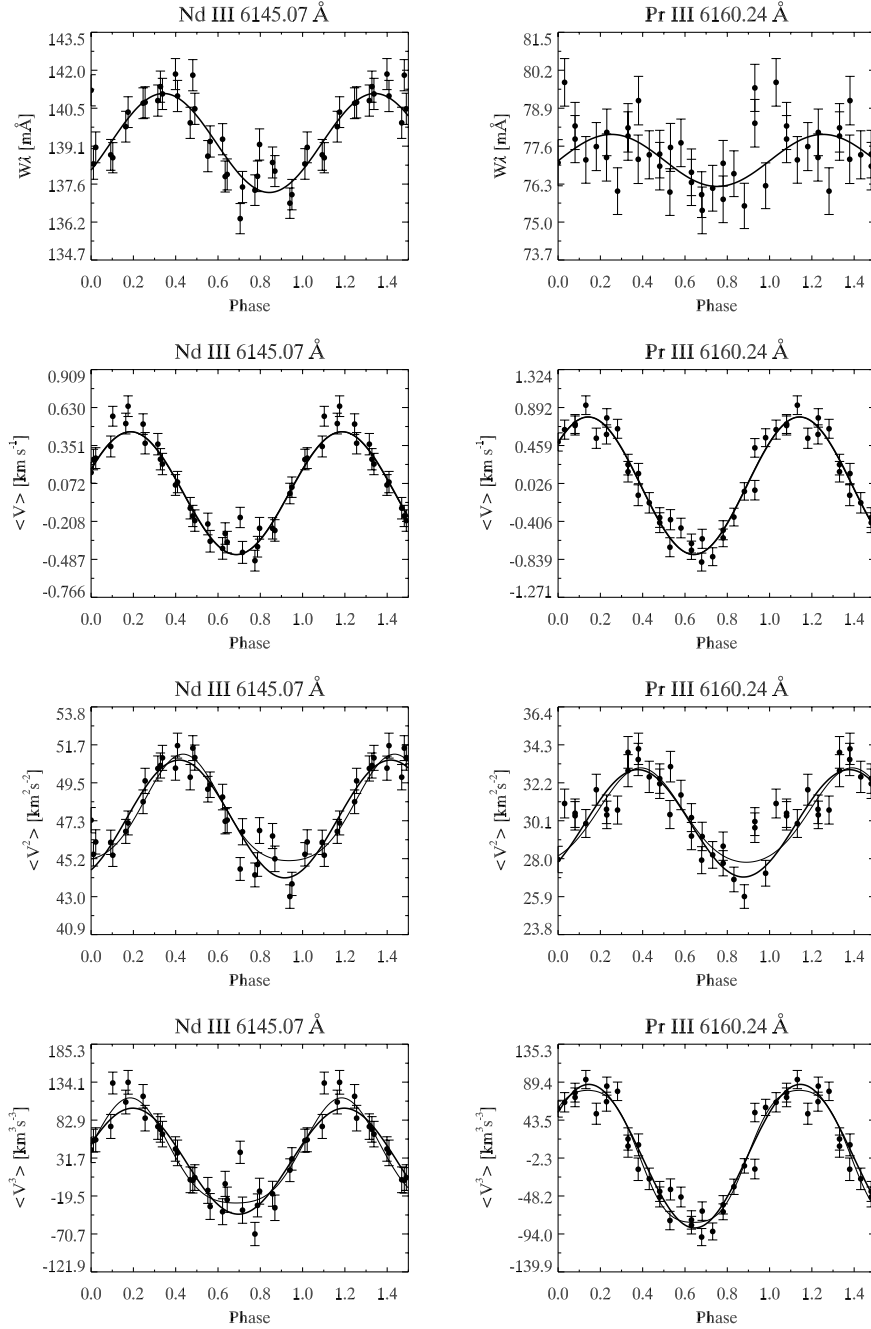
Fig. 4. Variation of the equivalent width and first three moments of Nd III 6145.07 Å and Pr III 6160.24 Å spectral lines. Thick line shows the fit by a cosine curve (7), while thin line on $\langle V^2 \rangle$ and $\langle V^3 \rangle$ panels illustrate the fit with formula (8).

the variation of the first three moments of a monoperiodic pulsation are given by:

$$
\begin{aligned}
\langle V \rangle &= A_{1,1} \sin(\omega t + \psi), \\
\langle V^2 \rangle &= A_{2,2} \sin(2\omega t + 2\psi + \tfrac{3\pi}{2}) \\
&\quad + A_{2,1} \sin(\omega t + \psi + \tfrac{3\pi}{2}) + A_{2,0}, \\
\langle V^3 \rangle &= A_{3,3} \sin(3\omega t + 3\psi) \\
&\quad + A_{3,2} \sin(2\omega t + 2\psi + \tfrac{3\pi}{2}) + A_{3,1} \sin(\omega t + \psi).
\end{aligned}
\tag{8}
$$

In these formulas ψ is the phase constant and the parameters $A_{n,k}$ depend on the type of the pulsation mode (ℓ and $|m|$ numbers), projected rotation velocity $v_{\mathrm{e}} \sin i$, pulsation velocity v_{p}, the angle between pulsation axis and line of sight and intrinsic stellar profile. The functions $A_{n,k}$ can be used to identify pulsation mode and are usually esti-

mated by considering periodograms of the three moments (Aerts et al. 1992). The small number of γ Equ observations precluded us from using this approach, instead we directly fitted the variations of all three moments with expressions (8) using the Marquardt method. Figure 4 compares this fit with the observations and a simple cosine approximation of the moment curves. The best-fit amplitudes $A_{n,k}$ and their formal errors are summarised in Table 2. Apparently variations of all four first moments of Nd III and Pr III lines are dominated by the fundamental pulsation frequency and our data do not give unambiguous support for the presence of the first and second harmonics of the main pulsation frequency in the variations of $\langle V^2 \rangle$ and $\langle V^3 \rangle$. Thus, amplitudes $A_{2,2}$, $A_{3,2}$ and $A_{3,3}$,

Table 2. Variation of the moments of doubly ionized REE lines parametrised by a cosine curve (7) (parameters K_n and φ_n) and by expressions (8) (parameters $A_{n,k}$). Amplitudes K_n ($n > 0$) and $A_{n,k}$ are given in units of $(\mathrm{m\,s^{-1}})^n$, where n is the moment order, while W_λ variations are given in mÅ units. Phases φ_n are expressed in units of the period.

Amplitude	Nd III 6145.07 Å			Pr III 6160.24 Å		
			zeroth moment: W_λ			
K_0	1.90	$\pm$	0.16	0.89	$\pm$	0.22
φ_0	0.342	$\pm$	0.013	0.253	$\pm$	0.039
			first moment: $\langle V \rangle$			
K_1	0.452	$\pm$	0.022	0.784	$\pm$	0.028
φ_1	0.187	$\pm$	0.007	0.143	$\pm$	0.006
$A_{1,1}$	0.452	$\pm$	0.020	0.784	$\pm$	0.024
			second moment: $\langle V^2 \rangle$			
K_2	3.36	$\pm$	0.19	2.99	$\pm$	0.22
φ_2	0.416	$\pm$	0.009	0.377	$\pm$	0.011
$A_{2,0}$	47.59	$\pm$	0.15	30.12	$\pm$	0.16
$A_{2,1}$	3.03	$\pm$	0.22	2.63	$\pm$	0.24
$A_{2,2}$	0.52	$\pm$	0.23	0.30	$\pm$	0.24
			third moment: $\langle V^3 \rangle$			
K_3	71.49	$\pm$	4.70	86.76	$\pm$	2.95
φ_3	0.197	$\pm$	0.009	0.146	$\pm$	0.006
$A_{3,1}$	71.15	$\pm$	4.70	86.11	$\pm$	2.91
$A_{3,2}$	13.15	$\pm$	4.53	1.77	$\pm$	3.12
$A_{3,3}$	0.22	$\pm$	4.41	6.33	$\pm$	2.94

given in Table 2, should be considered as the upper limits of these parameters. Longer and preferentially multi-site spectroscopic time-series are required for improving the phase curves of the second and third moments.

With the exception of Nd III 6145.07 Å and Pr III 6160.24 Å there are no other lines in the 6140–6166 Å spectral region that are suitable for accurate moment measurements. The other REE lines are weak and blended, while relatively unblended strong lines of lighter elements (Ba II 6141.71 Å, Fe II 6147.74 Å, Ca I 6162.17 Å, and Ca I 6163.76 Å) do not exhibit profile changes. Equivalent width variations at the level above 2 mÅ are also absent for these spectral lines.

5.2. Amplitudes and phases across line profiles

During an oscillation cycle the flux at every pixel of the line profile varies with the same period(s). Therefore one can apply the usual time-series analysis to the variations of the fluxes in individual pixels. In particular, Fourier frequency analysis with the CLEAN algorithm (e.g. De Mey et al. 1998) helps to extract periodicities present in the pulsation spectrum. For moderately and rapidly rotating non-radial pulsators such line profile analysis is also the only way to detect pulsation modes with high ℓ numbers, since these modes cancel out in disk-averaged observables such as centroid RV or brightness.

Limited time-series of profile variations (similar to out γ Equ data) are not well suited for the period determination, but can be efficiently analysed with the least-squares algorithm described by Mantegazza (2000). In this method

variation of the ith pixel is approximated by the superposition of n sinusoidal components, corresponding to n detected frequencies

$$f_i^j = F_i + \sum_{k=1}^{n} D_{i,k} \cos(2\pi t^j / P_k + \psi_{i,k}), \qquad (9)$$

where F_i, $D_{i,k}$, and $\psi_{i,k}$ are free parameters, optimized by the least-squares method assuming fixed set of periods P_k.

In the analysis of line profile variations of Nd III 6145.07 Å and Pr III 6160.24 Å we assumed that variations with a single period (P_2 for Nd III and P_1 for Pr III) are present and derived the estimate of the average line profile $F(\lambda)$ together with the variation of the pulsation amplitude $D(\lambda)$ and phase $\psi(\lambda)$ across the line profiles. Figure 5 shows these functions and their formal errors.

5.3. Mode identification

Unfortunately elaborate modelling techniques developed in recent years for the spectroscopic analysis of non-radial oscillations of normal stars are not directly applicable and cannot be easily adapted for roAp pulsations. In most of the studies of line profile variations in non-radially pulsating stars the pulsation axis is assumed to be aligned with the rotation axis. Therefore an inclination angle is one of the important parameters. In roAp stars a general model describing stellar pulsations is the oblique pulsator model (Kurtz 1982). According to this model the pulsation axis is aligned with the magnetic rather than the rotation axis. Hence, we have to use an inclination of the magnetic axis to the line of sight (angle α) instead of the usual inclination angle. As the star rotates the angle α varies and therefore the pulsation amplitudes are modulated with rotation period. This effect has to be properly taken into account in the analysis of rapidly rotating roAp stars, but with the extremely slow rotation of γ Equ we do not expect to see any rotational modulation of the pulsations and can treat the star as if it were a δ Scuti-type variable observed at inclination angle $i = \alpha$. Besides variable orientation of the pulsation axis, a strong magnetic field, which is present in the atmospheres of many roAp stars, alters the pulsation velocity field (e.g. Bigot et al. 2000) and simultaneously introduces Zeeman broadening and splitting of spectral lines. The latter effect makes a Gaussian approximation of the local line profile (Aerts et al. 1992; Schrijvers et al. 1997) highly questionable. Despite all these ambiguities, in this section we try to identify the pulsation mode of γ Equ applying methods developed for normal non-radial pulsators to the variation of Pr III and Nd III spectral lines. This semi-qualitative analysis should be regarded with caution and it by no means aspires to reach any definite conclusions about the pulsation velocity distribution in the atmosphere of γ Equ.

In principle diagrams that show the behaviour of the phases of each mode across the line profiles (Fig. 5) are able to discriminate between pulsation modes with
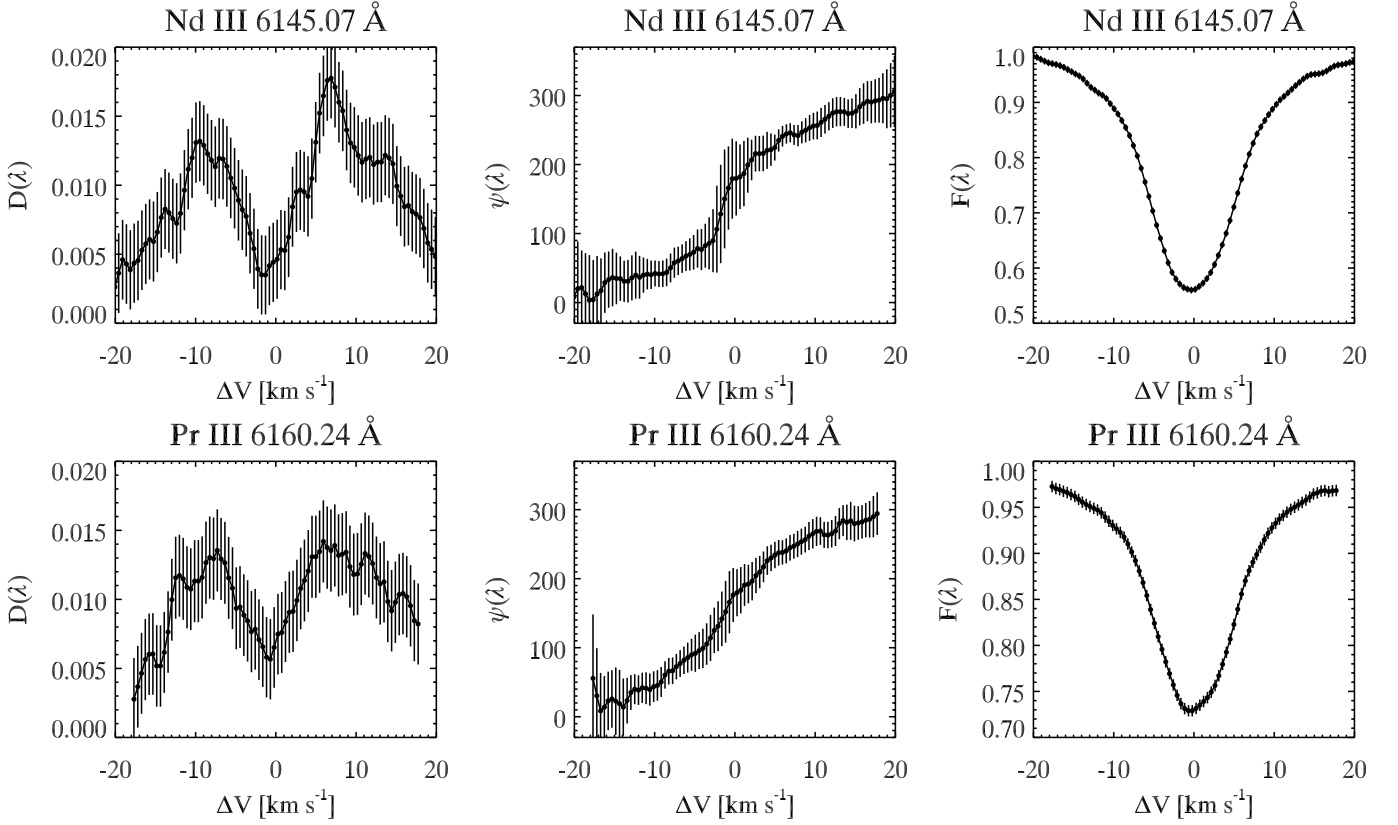
Fig. 5. Behavior of amplitudes (left panels) and phases (middle panels) across the profiles of Nd III 6145.07 Å and Pr III 6160.24 Å spectral lines. The bars are formal 1σ errors derived in a least-squares analysis of the profile variation. Phases $\psi(\lambda)$ are given in degrees, while amplitudes $D(\lambda)$ are in units of the continuum flux. The right panels show an estimate of the average line profile.

different ℓ and m. Telting & Schrijvers (1997) determined linear relations between the observed phase difference and mode parameters ℓ and $|m|$ for non-radially pulsating rotating stars. It is not correct to apply directly these relations for γ Equ because they were obtained for a rapidly rotating star, which is not fulfilled in our case. However we expect to get a lower limit for ℓ using the proposed method. From Telting & Schrijvers' Eq. (9) we get $\ell \approx 0.10 + 1.09|\Delta\psi_0|/\pi$, where $\Delta\psi_0$ is the blue-to-red phase difference for the variations with the main pulsation frequency (middle panels in Fig. 5). For both Pr III and Nd III lines $\Delta\psi_0 \approx 300°$ or 1.67π, therefore $\ell \gtrsim 2$.

A consideration of the shape of the amplitude and phase diagrams for individual spectral lines opens another possibility for mode identification. In particular, the similarity of our pixel-by-pixel amplitude and phase diagrams to those derived for 5.31 d^{-1} mode of δ Scuti-type variable HD 2724 (Mantegazza & Poretti 1998), for which $\ell = 2\pm1$ and $m = 2\pm1$ was obtained, allows us to propose $\ell \approx 2\pm1$ and $|m| \approx 2\pm1$ for the mode identification of the γ Equ RV pulsations. The sign of m depends on the angle α between line of sight and pulsation (magnetic) axis. This angle can be determined from the parameters of the γ Equ magnetic model suggested by Leroy et al. (1994). They found that published longitudinal and broadband linear polarisation magnetic observations can be fitted with a dipolar field $B_\mathrm{d} = 5.5$ kG and two combinations of inclination angle

i and angle β between the magnetic and rotation axes ($i = 150°$, $\beta = 80°$ and $i = 80°$, $\beta = 150°$). These two models yield the same α:

$$\cos\alpha = \cos i \cos\beta + \sin i \sin\beta \cos\Phi, \qquad (10)$$

where Φ is rotational phase. Assuming that the epoch of our γ Equ observations roughly corresponds to $\Phi = 0.8 \pm 0.1$ (see Leroy et al. 1994; Scholz et al. 1997), we find $\alpha = 132° \pm 10°$. This value of α together with the positive slope of the $\psi(\lambda)$ curves allows us to conclude that γ Equ pulsates in prograde mode (negative m).

An alternative possibility of mode identification comes from moment analysis through the comparison between the observed moment amplitudes and calculations for a set of parameters $\ell, m, i = \alpha, v_\mathrm{p}$ and variance σ of the intrinsic Gaussian stellar profile (Aerts et al. 1992; Aerts 1996). The most probable combination of $(l, m, \alpha, \sigma, v_\mathrm{p})$ can be defined as the one for which the weighted squared differencies between observed and calculated moment amplitudes,

$$Q = \sum_{n,k} (A_{n,k}^\mathrm{obs} - A_{n,k}^\mathrm{calc})^2/\sigma^2(A_{n,k}^\mathrm{obs}), \qquad (11)$$

reaches its minimal value. We calculated theoretical moment amplitudes $A_{n,k}^\mathrm{calc}$ using the code of Aerts (1996) and compared them with amplitudes $A_{n,k}^\mathrm{obs}$ of the first three moments determined for Nd III and Pr III lines in Sect. 5.1 (see

Table 3. Estimate of the width of Gaussian profile σ, pulsational velocity v_p (both are given in $\mathrm{km\,s^{-1}}$) and angle α (in degrees) for the three best-fit pulsation modes of γ Equ.

ℓ	$\lvert m\rvert$	Nd III 6145.07 Å			Pr III 6160.24 Å		
		σ	v_p	α	σ	v_p	α
3	3	5–6	8–14	130–160	4	7–8	120–130
2	2	6	10–11	160	3–5	5–14	140–160
3	2	6	7	100–160	3–4	7–9	110–150

Table 2). For the projected rotation velocity we adopted value $v_\mathrm{e}\sin i = 0.003\ \mathrm{km\,s^{-1}}$, estimated from the rotational period of 77 yr assuming the rigid rotation of γ Equ. Since angle α is relatively well constrained by the published model of the magnetic topology, we considered only the values of $\alpha = 130° \pm 30°$. The variance of the intrinsic Gaussian profile is another parameter required for the moment amplitudes calculation. The lower limit of this parameter (non-magnetic broadening effects) can be estimated from the width of the resolved Zeeman components of Fe II 6149.26 Å: both lines give $\sigma_{6149} = 2.6\ \mathrm{km\,s^{-1}}$. On the other hand the magnetic contribution to σ should be of the order of the separation of magnetic σ components, which for Nd III and Pr III lines amounts to an additional $\sigma_\mathrm{mag} \simeq 3\ \mathrm{km\,s^{-1}}$. Thus we adopted $\sigma \simeq 4 \pm 2\ \mathrm{km\,s^{-1}}$ for the calculation of the weighted sum (11). Table 3 summarises the parameters σ, v_p and α which give the lowest $Q(\mathrm{Nd\,III})+Q(\mathrm{Pr\,III})$ within the errors of the observed amplitudes $A_{n,k}^\mathrm{obs}$ for the three best-fit modes. Despite the relatively large scatter of v_p and α these results generally support a pulsational velocity $v_\mathrm{p} \approx 10\ \mathrm{km\,s^{-1}}$ and are consistent with the mode identification suggested above. Thus we conclude that the most probable parameters of the p-mode in γ Equ are $\ell = 2$ or 3 and $m = -\ell$ or $-\ell+1$.

6. Pulsational broadening of spectral lines

As we mentioned in Sect. 3 there exists an unexplained extra broadening of spectral lines in γ Equ. The pulsations themselves may introduce such a broadening. Hao (1998) noticed that the average line profile in the spectrum of pulsating stars is wider than in the spectrum of non-pulsating stars. M. Montgomery (private communication) calculated the line profile for $\ell = 1$, $m = 1$, $v_\mathrm{p} = 10.5\ \mathrm{km\,s^{-1}}$ in the spectrum of the δ Scuti-type variable FG Vir. This line profile corresponds to a synthesized one in a non-pulsating star with a macroturbulent broadening of $10\ \mathrm{km\,s^{-1}}$ (Mittermayer 2000). Figure 6 shows a comparison between the observed and computed γ Equ spectrum for two values of macroturbulence: 2 and $10\ \mathrm{km\,s^{-1}}$. A macroturbulence of $10\ \mathrm{km\,s^{-1}}$ is required to fit the Nd III and Pr III lines, while we need much lower macroturbulence to fit most of the other lines. Our pulsational velocity $v_\mathrm{p} \approx 10\ \mathrm{km\,s^{-1}}$, estimated from the Pr III and Nd III lines, is in a good agreement with the macroturbulent velocity inferred from these lines. The lower macroturbulence for other lines is consistent with the lower observable RV amplitudes. Of course, this effect should

be investigated for a larger number of roAp and related stars, but we may conclude that a study of differential macroturbulent-like line broadening may give us important information on RV pulsation amplitudes.

Non-radial RV oscillations can introduce a line broadening in the average spectrum through two main effects. First, in the process of coaddition of the line profiles with different RV shifts one produces an average spectrum which is somewhat wider than the individual line profiles. However, careful inspection of our γ Equ observations showed that the time-resolved profiles of Nd III and Pr III lines are not significantly sharper in comparison with the average spectrum. We suggest that the second broadening effect related to non-radial oscillations is responsible for the large observed width of doubly ionized REE lines. At any given pulsation phase the individual line profiles contain information about the velocity distribution on the stellar surface. If this velocity distribution is sufficiently inhomogeneous and the influence of the rotational Doppler broadening is negligible, individual time-resolved line profiles will appear broader in comparison with a non-pulsating star. Note that for a given pulsational velocity non-radial modes with lower ℓ numbers will produce higher amplitudes of RV variations, since in the case of slow rotation RV shifts due to higher ℓ modes will tend to cancel out more efficiently in the disk-integrated profiles. Thus, the very fact of significant broadening of Nd III and Pr III lines together with the value of the most probable pulsational velocity ($v_\mathrm{p} \approx 10\ \mathrm{km\,s^{-1}}$) and high RV amplitudes indicates that γ Equ pulsates in a dominant low-ℓ non-radial mode.

We performed a rough study of the influence of non-radial oscillations on the shape of average line profiles using the code `lnprof2` developed by Balona (2000). This programme makes it possible to calculate line profile variations of non-radially pulsating star due to the changes in local RV, temperature and gravity under the assumption of a constant intrinsic local line profile. This simplification is definitely not correct for roAp stars for which we expect the local line profile to undergo strong changes from one point on the stellar surface to another due to the variations of the local elemental abundance as well as magnetic field strength and direction. These complications associated with the nature of magnetic Ap stars preclude us from directly fitting the line profile variations using `lnprof2`. Nevertheless, Balona's code is useful to illustrate the pulsation broadening of average line profiles described above. In the lower panels of Fig. 6 we compare high-resolution observations of Nd III and Pr III lines with average synthetic line profiles computed by `lnprof2` for sectoral modes with $\ell = 2$ and $\ell = 4$, $\alpha = 130°$ and $v_\mathrm{p} = 10\ \mathrm{km\,s^{-1}}$. For the intrinsic local profile we adopted synthetic disk-average `Synthmag` spectra (dashed line in lower panels of Fig. 6) broadened by Gaussian with $FWHM = 1.8\ \mathrm{km\,s^{-1}}$ to take into account instrumental effects. Figure 6 shows that including non-radial pulsations allows us to improve the agreement between spectrum synthesis and observations. (The discrepancy
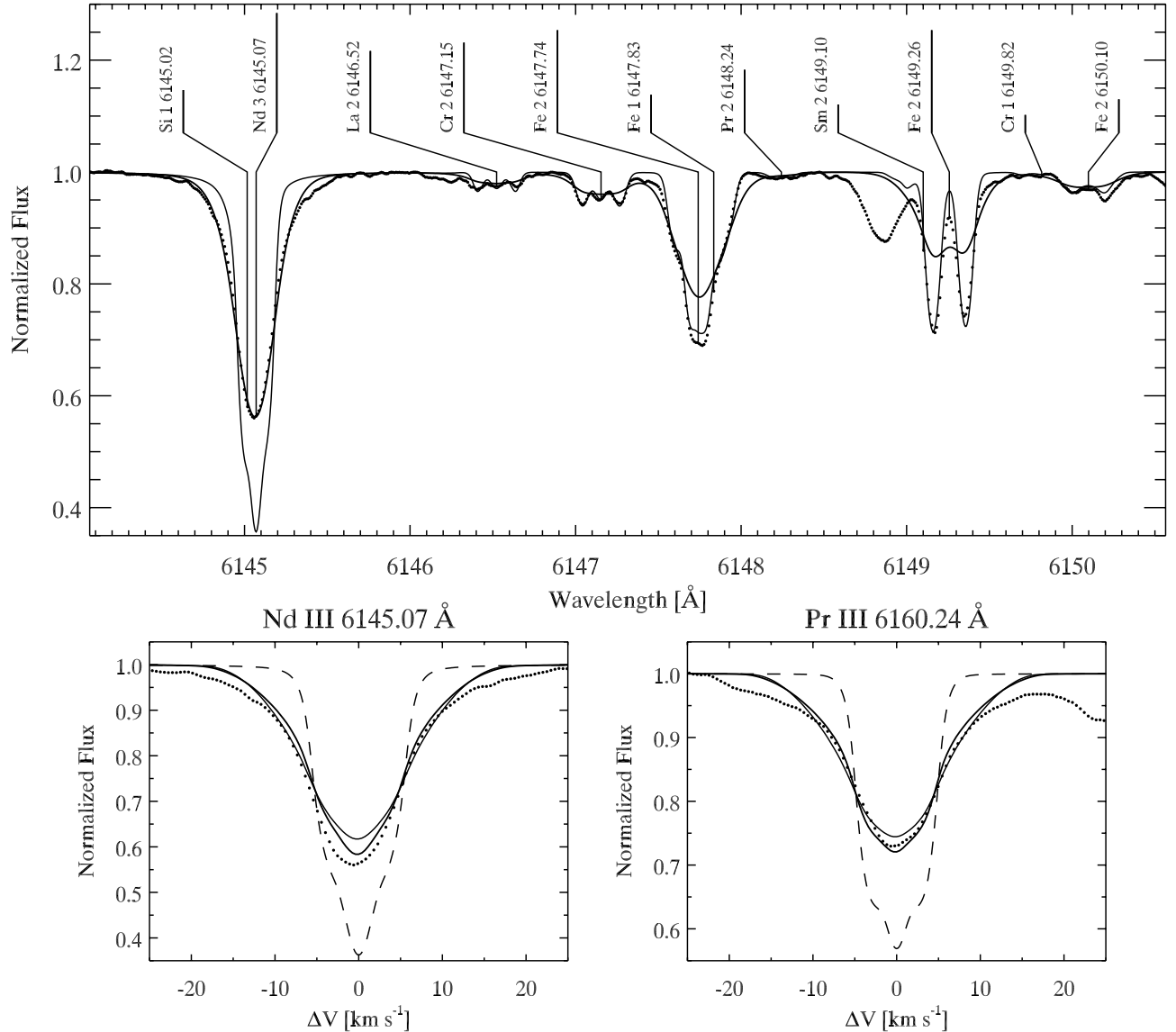
Fig. 6. The upper panel shows a comparison between observations (dots) and synthetic spectrum calculations for two macro-turbulent velocities: 2 km s^{-1} (thin line) and 10 km s^{-1} (thick line). The lower panels illustrate the effect of pulsations with sectoral $\ell = 2$ (thin line) and $\ell = 4$ (thick line) modes as seen in the average profiles of doubly ionized REE lines. The observed spectrum is shown by dots, while the dashed line corresponds to the synthetic profiles in the absence of pulsations.

between observations and synthetic spectra seen in the blue wing of Nd III 6145.07 Å line is due to the blending by Si I 6145.02 Å, which cannot be included in the local intrinsic profile and broadened by $v_\mathrm{p} = 10$ km s^{-1} because we do not observe strong RV variations for other Si I lines.) In general we found that the width of the average profiles broadened by pulsations is rather insensitive to the pulsation mode, but shows strong dependence on v_p and α, which again supports the idea that v_macro, required to fit doubly ionized REE lines in γ Equ spectrum, provides a useful estimate of the pulsation velocity amplitude.

7. Discussion

Based on high-resolution high S/N observations we confirmed earlier results obtained by Savanov et al. (1999),

who discovered strong RV variations of doubly ionized REE lines in the spectrum of γ Equ. In addition to refining the measurements of variations of the third REE ions, we were also able to obtain precise radial velocity amplitudes and phases for singly ionized REE. Our data give an indication for the existence of a phase lag of ≈80° between RV variations of singly (average phase $\langle\varphi\rangle = 0.935 \pm 0.053$) and doubly ionized ($\langle\varphi\rangle = 0.160 \pm 0.009$) REE. The lines of all other elements but Na I do not show RV variations with amplitudes greater than 100 m s^{-1}. Below this threshold some RV variations are possible for Fe II lines and are definitely present for Ba II line (which varies in phase with singly ionized REE), while strong Ca I lines are stable to within 30–50 m s^{-1}. These amplitudes are consistent with earlier RV analyses (Libbrecht 1988; Kanaan & Hatzes 1998).
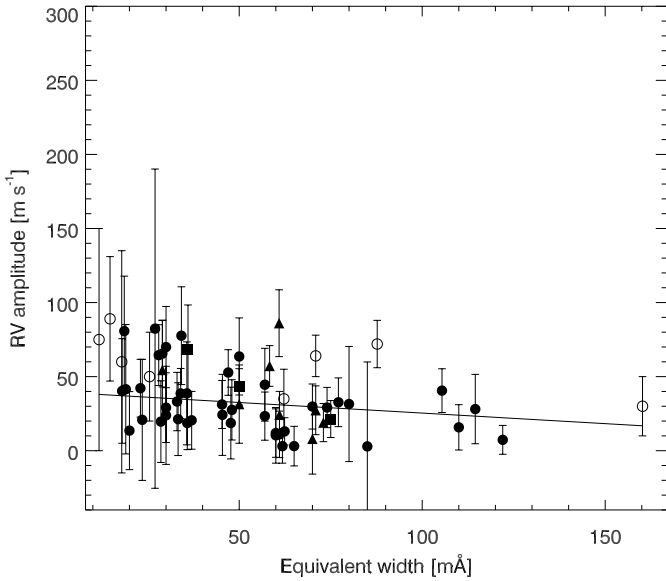
Fig. 7. Amplitudes of RV variations of spectral lines shown as a function of equivalent width. Filled symbols correspond to unblended lines of Fe (circles), Cr (triangles) and Ti (squares) from the study of Kanaan & Hatzes (1998), while open circles represent results of our study for all lines except Ba II, Na I and REE. The solid line shows a weighted least-squares fit by a straight line Amp $= a \cdot EW + b$ ($a = -0.14 \pm 0.07$, $b = 39.66 \pm 5.31$, $\chi^2 = 69.6$). The low χ^2 probability of this linear fit ($P(\chi^2) = 18.5\%$) together with the value of the weighted linear correlation coefficient $r = -0.16$ and the relatively high false-alarm probability $P(r) = 20.1\%$ indicate the absence of significant correlation.

We did not confirm a correlation of the RV amplitudes with the line intensity found in the latter paper. Looking through the line list published by Kanaan & Hatzes we found that many spectral lines with high RV amplitudes were not identified properly and in reality belong to REE lines in different ionization stages. We performed a careful spectral synthesis of all lines published by Kanaan & Hatzes (1998) with the best atmospheric abundances of γ Equ to check for blending effects. First, blends with REE lines were removed from Kanaan & Hatzes' list of Ti, Cr and Fe lines. Next, a few lines were found to be too strong or shifted in wavelength for the proposed identification ($\lambda\lambda$ 5151.84, 5566.00, 6044.50, 5379.00 Å). The first two unidentified lines are very strong in the famous, extremely REE-rich, Fe-weak Przybylski's star (HD 101065 – see line identification list from Cowley et al. 2000), which provides additional evidence for their wrong identification by Kanaan & Hatzes. Finally 54 out of 70 lines of Ti, Cr and Fe were chosen as unblended or partially blended by the same species. We add 8 lines of Ca, Cr and Fe from our study and plot RV amplitudes versus equivalent widths in Fig. 7. There is no statistically significant correlation between line intensity and pulsational amplitude.

Taking into account our results we looked through RV pulsational analyses of α Cir (Baldry et al. 1998a, 1999) and HD 83368 (Baldry et al. 1998b; Baldry & Bedding 2000). Low resolution spectra were used for both stars. There are 24 spectral regions in α Cir with RV amplitudes higher than 150 m s^{-1} and exceeding three individual rms estimates. The lines of doubly ionized REE are identified in 9 of them. Two telluric bands, 6864–6881 Å and 6903–6920 Å, used as a fiducial reference for Hα RV analysis, contain rather strong Pr III lines, 6866.73 Å and 6910.15 Å. The influence of the last line on RV analysis is easily seen, because a phase of the band (263°) is close to the phases of the bands with other Pr III and Nd III lines (e.g. band 18 with Pr III 6195.63 Å and band 33 with Nd III 6327.27 Å lines, see Table 3 in Baldry et al. 1998a). Strong RV variations of REE lines may also be responsible for producing small phase difference between light and Hα RV variations found by Baldry et al. (1998b) for HD 83368. A presence of strong Nd III 6550.33 Å line in the blue wing of Hα is the most probable reason for the jump in amplitude and phase near the intensity 0.8 of Hα in α Cir (Baldry et al. 1999). Our knowledge of the second spectra of the REE is very scarce, therefore it will not be surprising if their future identification will explain a significant part of the observational features of the roAp stellar pulsations. A weak correlation between line intensity and RV pulsational amplitude found by Baldry et al. (1998a) in α Cir can be easily explained by the low spectral resolution of their observations.

The fact that the lines of the second ions of Pr and Nd show the highest pulsational amplitudes in roAp stars was supported by the recent time-series analysis of another roAp star HD 83368 (Baldry & Bedding 2000). Six out of eight spectral bands with metallic lines presented in their Table 4, which show the highest amplitudes of RV pulsations (Nos. 13, 14, 18, 33, 54, 90), contain known spectral lines of Pr III and Nd III. It is important to note that RV amplitudes are higher for those bands where Pr III and Nd III lines contribute more than 60% to the total band intensity (Nos. 18 and 33), while RV amplitudes of the bands where contribution of Pr III and Nd III lines is less than 30% (Nos. 13, 14, 54) are smaller. Rather strong lines of iron-peak elements with low RV amplitudes in these bands decrease the net value of the RV amplitude derived by cross-correlation analysis of low resolution spectra.

Weiss et al. (2000) and Ryabchikova et al. (2001) analysed Pr III and Nd III lines in the spectra of a dozen roAp and non-pulsating Ap stars and found that for roAp stars elemental abundances obtained from Pr III and Nd III lines are up to two orders of magnitude higher than abundances derived from the lines of singly ionized Pr and Nd. In non-pulsating Ap stars the same anomaly is marginal if present at all. Ryabchikova et al. (2001) proposed that REE are concentrated in the uppermost atmospheric layers where a transition from singly to doubly ionized REE occurs due to a pressure drop. Unfortunately no quantitative diffusion calculations are available for the REE. However, qualitatively, proposed REE distribution is supported by diffusion calculations for another heavy element, Hg (Michaud et al. 1974). An analysis of the abundance stratification in the atmosphere of γ Equ and the distribution of the

pulsational amplitudes will be given in a separate paper. The phase shifts of RV variations (cf. Na I, singly and doubly ionized REE) as well as the amplitude difference may be connected with inhomogeneous surface and vertical abundance and pulsation amplitude distributions or indicate non-adiabatic pulsations. The extremely slow rotation of γ Equ does not allow us to investigate the distribution of the different elements over the surface of the star and correlate it with pulsation amplitudes, but at least two other roAp stars, HD 24712 (Ryabchikova et al. 2000) and HD 83368 (Polosukhina et al. 2000), are known to be spotty pulsators. The latter star is of particular interest for simultaneous time-resolved photometry and spectroscopy over the rotational period due to its substantial rotation.

An application of the relation between velocity and luminosity amplitudes for the solar-like p-mode oscillations to δ Scuti and roAp stars was discussed by Kjeldsen & Bedding (1995). If we adopt the pulsational amplitude of approximately 100 m s^{-1} in the atmosphere of γ Equ, as it follows from the lines of iron-peak elements, Si I and Ba II, and effective temperature of 7700 K (Ryabchikova et al. 1997), we get a prediction for the light variation amplitude of about 1.3 mmag at 440 nm (Johnson B) using Eq. (5) of Kjeldsen & Bedding (1995). This value agrees reasonably well with the semi-amplitude of 0.5–1.3 mmag observed for γ Equ by Kurtz (1983). But if we apply the pulsational amplitude of 500 to 800 m s^{-1} as derived from Nd III and Pr III lines then the expected light variation amplitude would be greater than 6.0 mmag. Either the relation between velocity and luminosity amplitudes is not valid for roAp stars or high amplitude RV pulsations occur in the atmospheric layers whose contribution to the total luminosity is negligible.

References

Aerts, C., De Pauw, M., & Waelkens, C. 1992, A&A, 266, 294
Aerts, C. 1996, A&A, 314, 115
Babel, J. 1992, A&A, 258, 449
Baldry, I. K., Bedding, T. R., Viskum, M., Kjeldsen, H., & Frandsen, S. 1998, MNRAS, 295, 33
Baldry, I. K., Kurtz, D. W., & Bedding, T. R. 1998, MNRAS, 300, L39
Baldry, I. K., Viskum, M., Bedding, T. R., Kjeldsen, H., & Frandsen, S. 1999, MNRAS, 302, 381
Baldry, I. K., & Bedding, T. R. 2000, MNRAS, 318, 341
Balona, L. A. 1986a, MNRAS, 219, 111
Balona, L. A. 1986b, MNRAS, 220, 647
Balona, L. A. 2000, in Delta Scuti and Related Stars, ed. M. Breger, & M. H. Montgomery, ASP Conf. Ser., 210, 170
Bevington, P. R. 1969, Data reduction and Error analysis for the physical sciences (Mc Graw-Hill Book Company)
Bigot, L., Provost, J., Berthomieu, G., Dziembowski, W. A., & Goode, P. R. 2000, A&A, 356, 218
Cowley, C. R., Ryabchikova, T. A., Kupka, F., et al. 2000, MNRAS, 317, 299
De Mey, K., Daems, K., & Sterken, C. 1998, A&A, 336, 327
Hao, J. 1998, ApJ, 500, 440
Horne, J. H., & Baliunas, S. L. 1986, ApJ, 302, 757
Kanaan, A., & Hatzes, A. P. 1998, ApJ, 503, 848
Kjeldsen, H., & Bedding, T. R. 1995, A&A, 293, 87
Kupka, F., Piskunov, N., Ryabchikova, T. A., Stempels, H. C., & Weiss, W. W. 1999, A&AS, 138, 119
Kurtz, D. W. 1982, MNRAS, 200, 807
Kurtz, D. W. 1983, MNRAS, 202, 1
Kurtz, D. W., & Wegner, G. 1979, ApJ, 232, 510
Kurucz, R. L., Furenlid, I., Brault, J., & Testerman, L. 1984, NSO Atlas No. 1: Solar Flux Atlas from 296 to 1300 nm, Sunspot, NSO
Leroy, J. L., Bagnulo, S., Landolfi, M., & Landi Degl'Innocenti, E. 1994, A&A, 284, 174
Libbrecht, K. G. 1988, ApJ, 330, L51
Malanushenko, V., Savanov, I., & Ryabchikova, T. 1998, IBVS, No. 4650
Mantegazza, L. 2000, in Delta Scuti and Related Stars, ed. M. Breger, & M. H. Montgomery, ASP Conf. Ser., 210, 138
Mantegazza, L., & Poretti, E. 1998, A&A, 312, 855
Martinez, P., Weiss, W. W., Nelson, M. J., et al. 1996, MNRAS, 282, 243
Michaud, G. 1970, ApJ, 160, 641
Michaud, G., Reeves, H., & Charland, Y. 1974, A&A, 37, 313
Mittermayer, P. 2000, Master Thesis, University of Vienna
Mkrtichian, D. E., Samus, N. N., Gorynya, N. A., et al. 1998, IBVS, 4564
Piskunov, N. E. 1999, in 2nd Workshop on Solar Polarization, ed. J. Stenflo, & K. N. Nagendra (Kluwer Academic Publishers, Dordrecht), 515
Polosukhina, N. S., Shavrina, A. V., Hack, M., et al. 2000, A&A, 357, 920
Ryabchikova, T. A., Adelman, S. J., Weiss, W. W., & Kuschnig, R. 1997, A&A, 322, 234
Ryabchikova, T. A., Tsymbal, V. V., Malanushenko, V. P., & Savanov, I. S. 2000, in Magnetic Fields of Chemically Peculiar and Related Stars, ed. Yu. V. Glagolevskij, & I. I. Romanyuk, Moscow, 180
Ryabchikova, T. A., Savanov, I. S., Malanushenko, V. P., Kudryavtsev, D. O. 2001, Astron. Rep., 45, 382
Savanov, I. S., Malanushenko, V. P., & Ryabchikova, T. A. 1999, Astron. Lett., 25, 802
Scholz, G., Hildebrandt, G., Lehmann, H., & Glagolevskij, Y. V. 1997, A&A, 325, 529
Schrijvers, C., Telting, J. H., Aerts, C., Ruymaekers, E., & Henrichs, H. F. 1997, A&AS, 121, 343
Telting, J., & Schrijvers, C. 1997, A&A, 317, 723
Weiss, W. W., Ryabchikova, T. A., Kupka, F., et al. 2000, in Impact of large-Scale surveys on Pulsating Star Research, ed. L. Szabados, & D. W. Kurtz, ASP Conf. Ser., 203, 487